Polymer 50 (2009) 2958–2966

Contents lists available at ScienceDirect

Polymer

journal homepage: www.elsevier.com/locate/polymer

Supramolecular self-assembly through inclusion complex formation between poly(ethylene oxide-*b*-*N*-isopropylacrylamide) *block* copolymer and α-cyclodextrin

Cheng-Wei Tu [a], Shiao-Wei Kuo [b,**], Feng-Chih Chang [a,*]

[a] Institute of Applied Chemistry, National Chiao-Tung University, 30050 Hsinchu, Taiwan
[b] Department of Materials and Optoelectronic Science, Center for Nanoscience and Nanotechnology, National Sun Yat-Sen University, Kaohsiung, Taiwan

ARTICLE INFO

Article history:
Received 6 February 2009
Received in revised form
20 April 2009
Accepted 21 April 2009
Available online 3 May 2009

Keywords:
Cyclodextrin
Inclusion complexes
Block copolymer

ABSTRACT

A well-defined poly(ethylene oxide-*block*-*N*-isopropylacrylamide) (PEO-*b*-PNIPAM) diblock copolymer was synthesized by atom transfer radical polymerization and formed the inclusion complexes (ICs) after selective threading of the PEO segment of the block copolymer through the cavities of α-cyclodextrin (α-CD) units. The formation of the α-CD/PEO ICs between α-CD and PEO segment of the PEO-*b*-PNIPAM transformed the system from its original random coil conformation into a rod/coil-like structure. The stacking of the α-CD/PEO ICs and phase separation within the α-CD/PEO-*b*-PNIPAM IC resulted in the self-assembly of long-range-ordered lamellar structure exhibiting alternating layers of (i) α-CD/PEO ICs with hexagonally packed plates and (ii) amorphous phase of unincluded PEO/PNIPAM with brush conformation.

1. Introduction

Supramolecular polymer chemistry has emerged as a fascinating subject within macromolecular research in recent years. A number of unique supramolecular architectures, such as polyrotaxanes based on inclusion complexes (ICs) of cyclic host materials and threaded guest molecules, have been reported as novel polymeric assemblies [1]. Cyclodextrins (CDs) have been the most popular host molecules employed to construct such molecular assemblies. CDs are cyclic oligosaccharides consisting of six (α), seven (β), or eight (γ) glucose units linked by 1,4-α-glycosidic bonds [2]. They have a rigid, shallow truncated cone shape with a hydrophilic exterior and a hydrophobic interior cavity. The average diameters of the cavities of α-, β- and γ-CD are 4.5, 7.0, and 8.5 Å, respectively, while the height of each CD's torus is ca. 7.8 Å [3,4]. The cone-shaped cavities of CDs can act as hosts for a great variety of molecular guests [5]. The driving forces for IC formation are through a combination of geometric compatibility, van der Waals forces, and hydrophobic interactions between the CD cavity and the guest molecules [6,7]. Another important stabilizing force leads to the formation of ICs is hydrogen bonding between the hydroxyl groups situated along the rim of neighboring CDs [8,9]. Harada and Kamachi reported the first example of an IC formed via the self-assembly of α-CD and poly(ethylene glycol) [10]. Since this initial discovery of CD/polymer ICs, many other linear polymeric guests possessing either hydrophilic or hydrophobic properties have been reported to form ICs with various types of CDs [11–14]. Recently, a large number of publications have emerged describing the changes in the miscibility [15–17], crystallizability [18–20], and microdomain structures [21] of various polymers after formation of their respective CD ICs via selective threading onto guest segments. For example, a well-defined supramolecular structure for the α-CD ICs with linear poly(ethylene glycol) [22–24] and poly(ε-caprolactone) forms three-dimensional hexagonal crystal structures after reorganization through selective solvent treatment [22]. Zhu et al. have reported that the self-assembly process involves a gradual transition from an amorphous globule to a unique lamellar morphology consisting of stacked polypseudorotaxane bundles and amorphous polyether layers [25].

Although many guest polymers have been investigated for their interactions with various CDs, little attention has been paid to the changing morphologies of block copolymers after the formation of CD-based ICs. In a previous study, we found that the crystalline ICs formed from CDs and poly[(ethylene oxide)-*ran*-(propylene oxide)]-*block*-(γ-benzyl-L-glutamate) [P(EO-*r*-PO)-*b*-PBLG] displays a bilayer-like structure possessing both hexagonally packed

* Corresponding author. Tel./fax: +886 3 5131512.
** Corresponding author. Fax: +886 7 5254099.
E-mail addresses: kuosw@faculty.nsysu.edu.tw (S.-W. Kuo), changfc@mail.nctu.edu.tw (F.-C. Chang).

0032-3861/$ – see front matter © 2009 Elsevier Ltd. All rights reserved.
doi:10.1016/j.polymer.2009.04.034

polypeptide and channel-type columnar IC stacks [12]. Herein, we report the selective threading of α-CDs onto one segment of the block copolymer that is able to induce micro-phase separation and changes their microdomain morphology in the bulk state. The block copolymer used in this study is poly(ethylene oxide-*block*-*N*-isopropylacrylamide) (PEO-*b*-PNIPAM). This copolymer is almost miscible in its bulk state without forming self-assembly structure. α-CD units can thread over the PEO segment but not the PNIPAM segment of the block copolymer because of the steric hindrance of the *N*-isopropyl amide side groups. The formation of the ICs between α-CD and PEO segment of the PEO-*b*-PNIPAM shifts the conformation from a random coil into a rod/coil-like system. The threaded segments of the α-CD-based ICs tend to aggregate to form hexagonally packed crystals which inhibit the original compatibility of the copolymer and form a micro-phase separated morphology. Wide-angle X-ray diffraction (WAXD) and small-angle X-ray scattering (SAXS) of the α-CD/PEO-*b*-PNIPAM IC reveal that a lamellar structure of alternating layers of (i) α-CD/PEO ICs with hexagonally packed plates and (ii) amorphous phase of unincluded PEO/PNIPAM with brush conformation.

2. Experimental section

2.1. Materials

Polyethylene glycol monomethyl ether (PEO-OH) ($M_w = 2000$, PDI = 1.05) was purchased from Fluka. *N*-Isopropylacrylamide (NIPAM) (Japan TCI Chemical Co.) was purified by recrystallization from benzene/*n*-hexane and drying under vacuum for 24 h. Cupper(I) bromide, ethyl 2-bromoisobutyrate, and 2-bromoisobutyryl bromide were purchased from Acros Organics. Tris[2-(dimethylamino)ethyl]amine (Me_6TREN) was synthesized according to reported procedure [26]. α-Cyclodextrin (α-CD) was purchased from Japan TCI Chemical Co. Toluene and isopropyl alcohol (IPA) were purified by refluxing and distilling over CaH_2 before use. All other solvents and analytical reagents were purchased from commercial suppliers and used as received without further purification. All other solvents and analytical reagents were purchased from commercial suppliers and used as received without further purification.

2.2. Procedure

2.2.1. General procedure for the synthesis of the PNIPAM homopolymer

A 100-mL dried Schlenk flask containing a magnetic stirrer bar was charged with Cu(I)Br (14.3 mg, 0.1 mmol) and NIPAM (1.35 g, 12 mmol). After filling the flask with argon, IPA (3 mL) was added and the solution stirred for 10 min at room temperature. The mixture was degassed three times using a freeze–pump–thaw cycle and then it was vigorously stirred at 0 °C. After complete degassing, Me_6TREN (23.0 mg; 0.1 mmol) was injected into the solution via syringe. After 10 min, ethyl 2-bromoisobutyrate (19.5 mg; 0.1 mmol) was injected into the solution to initiate the reaction. The mixture was heated at 50 °C for 12 h and then evaporated to dryness under vacuum. The residue was diluted with tetrahydrofuran (THF) and then passed through an alumina column to remove the copper catalyst. The product was precipitated from ether three times and dried under vacuum overnight at room temperature to obtain the polymer as a white powder.

2.2.2. Preparation of macroinitiator PEG-Br [27]

PEO-OH (10.0 g, 5 mmol) was dissolved in 150 mL dried toluene in a 500-mL three-neck flask and azeotropic distillation was conducted to remove trace of water. Triethylamine (1.05 mL, 7.5 mmol) was added and the solution mixture was cooled to 0 °C. The solution of 2-bromoisobutyryl bromide (0.93 mL, 7.5 mmol) diluted in toluene (10 mL) was added dropwise over 30 min to the reaction flask via a dropping funnel. The reaction mixture was magnetically stirred overnight at room temperature and then filtered to remove the resultant salts. Most of the toluene was removed through rotary evaporation prior to precipitation into a 10-fold excess of hexane. The crude polymer obtained was dissolved in water at pH 8–9 and then extracted with dichloromethane. The organic layer was dried with anhydrous $MgSO_4$, filtered and concentrated using a rotary vacuum evaporator. The resultant polymer was then re-precipitated again in hexane and collected as the purified PEG-Br macroinitiator.

2.2.3. General procedure for the synthesis of the PEO-b-PNIPAM diblock copolymer

A 100-mL dried Schlenk flask containing a magnetic stirrer bar was charged with PEO-Br (1.0 g, 0.5 mmol), Cu(I)Br (71.7 mg, 0.5 mmol), and NIPAM (10.0 g, 70.7 mmol). Once filled with argon, an appropriate amount of 50:50 (v/v) IPA/water mixture was added and the solution stirred for 10 min at room temperature. The mixture was degassed three times using a freeze–pump–thaw cycle and then it was vigorously stirred at 0 °C. After complete degassing, Me_6TREN (115.2 mg, 0.5 mmol) was injected into the solution via syringe. Polymerization was performed at 0 °C (ice batch) for 12 h. The resultant solution was first evaporated to dryness under vacuum. The residue was diluted with THF and passed through an alumina column to remove the copper catalyst. The product was precipitated from ether three times and then dried under vacuum overnight at room temperature to produce the block copolymer as a white powder.

2.2.4. Preparation of α-CD/PEO-b-PNIPAM inclusion complexes

A solution of PEO-*b*-PNIPAM (1.13 g, 2.98 mmol of PEO repeat units) in H_2O (5 mL) was added dropwise with stirring to a solution of α-CD (1.45 g, 1.49 mmol) in H_2O (5 mL). The mixture was agitated ultrasonically for 1 h and then it was vigorously stirred for 24 h at room temperature. The white precipitate was separated by centrifugation, dried under vacuum, swelled with a small portion of distilled water for 10–15 s to dissolve the free polymer and uncomplexed α-CD, and then collected again via centrifugation. The product was dried overnight in vacuum, and then vigorously stirred in large amount of THF (0.5 g/50 mL) for 12 h to reorganize the precipitate. The dispersed product in THF was collected by filtration and dried in a vacuum oven at room temperature for 24 h.

2.3. Characterizations

The molecular weight and molecular weight distribution were determined by gel permeation chromatography (GPC) using a Waters 510 HPLC-equipped with a 410 differential refractometer, a refractive index (RI) detector, and three Ultrastyragel columns (100, 500, and 10^3 Å) connected in series in order of increasing pore size. DMF was the eluent at a flow rate of 1 mL/min. The molecular weight calibration curve was obtained using PEO standards. ^{1}H NMR spectra were recorded in DMSO-d_6 or $CDCl_3$ on a Bruker AM 500 (500 MHz) spectrometer, using the solvent signal as an internal standard. High-resolution solid state ^{13}C NMR spectra were recorded at room temperature using a Bruker DSX-400 spectrometer operated at a resonance frequency of 100.47 MHz. Spectra acquired using the cross-polarization (CP)/magic angle spinning (MAS)/high-power dipolar decoupling technique, with a 90° pulse width of 3.9 μs, a pulse delay time of 3 s, an acquisition time of 30 ms, and 2048 scans. A magic-angle sample-spinning rate of 5.4 kHz was used to avoid absorption overlapping. Differential scanning calorimetry (DSC) of the materials was performed under a continuous nitrogen purge (60 mL/min) using a TA Instruments DSC Q20. All samples were first heated to 180 °C, maintained isothermally for

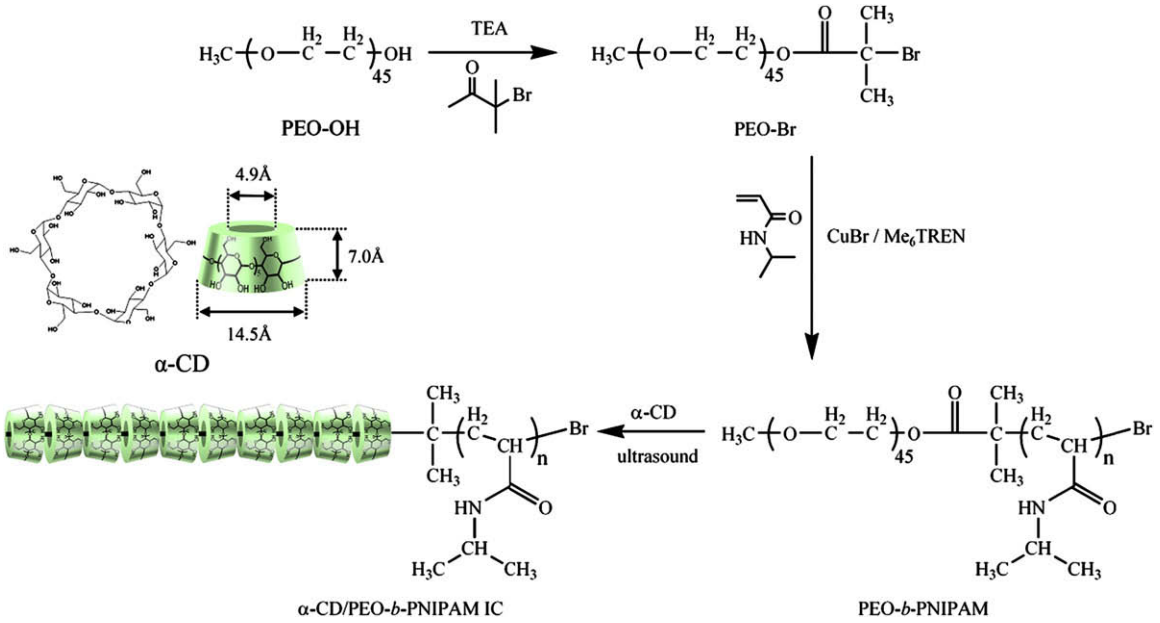

Scheme 1. Strategy for the preparation of the α-CD/PEO-*b*-PNIPAM IC.

5 min, and then quenched to −90 °C. Data were gathered on the second heating cycle at a scan rate of 20 °C/min over the temperature ranging from −90 to 200 °C. The glass transition temperature (T_g) was taken as the midpoint of the heat capacity transition between the upper and lower points of the deviation from the extrapolated glass and liquid lines. Thermal gravimetric analyses (TGA) were performed under nitrogen using a TA Instruments TGA Q50 thermal gravimetric analyzer operated at a heating rate of 20 °C/min over the temperature range from room temperature to 800 °C. The nitrogen or air flow rate was 40 mL/min. Wide-angle X-ray diffraction (WAXD) spectra were recorded from powdered samples using a Rigaku D/max-2500 type X-ray diffractometer. The radiation source used was Ni-filtered, Cu Kα radiation (wavelength = 0.154 nm). The voltage was set at 30 kV and the current at 20 mA. The sample was mounted on a circular sample holder; the proportional counter detector collected data at a rate of $2\theta = 5°$/min over the 2θ range 3.5–40°. Small-angle X-ray scattering (SAXS) experiments were performed using the SWAXS instrument at the BL17B3 beamline of the National Synchrotron Radiation Research Center (NSRRC), Taiwan. The X-ray beam having a diameter of 0.5 mm and a wavelength (λ) of 1.3329 Å was employed for the SAXS measurement. The samples of 1 mm thickness in general were sealed between two thin Kapton windows (80 μm in thickness) and measured at room temperature.

Table 1
Molecular weight characteristics of the macroinitiator, PNIPAM, and PEO-*b*-PNIPAM block copolymer.

Composition	Yield[a] (%)	M_w[b]	M_n[b]	M_w/M_n[b]	nNMR[c]	M_n[d]	Composition of PNIPAM[c] (wt%)
PEO_{45}-Br		1850	1790	1.03		2200	
$PNIPAM_{90}$	73	11,910	10,530	1.13	90	10,210	100
PEO_{45}-*b*-$PNIPAM_{128}$	82	13,440	11,470	1.17	128	16,680	87

[a] Isolated yield, after precipitation and drying.
[b] From GPC experiments performed using samples dissolved in DMF.
[c] Number-average degree of polymerization of the NIPAM segment, determined from ^{1}H NMR spectroscopy (DMSO-d_6).
[d] Number-average molecular weights of the diblock copolymer, characterized from ^{1}H NMR spectroscopic functional groups analysis.

3. Results and discussion

3.1. Spectroscopic analysis

3.1.1. Syntheses and characterizations of PEO-block-PNIPAM diblock copolymers

Scheme 1 presents the procedure employed for the synthesis of the α-CD/PEO-*b*-PNIPAM IC. The haloid-tailed PEO-Br was first prepared through esterification of the polyethylene glycol monomethyl ether (PEO-OH). The PEO-*b*-PNIPAM was then synthesized via the ATRP of *N*-isopropylacrylamide (NIPAM) using the haloid-tailed PEO-Br as the macroinitiator. The resulting macroinitiator and block copolymer were characterized by ^{1}H NMR spectroscopy and GPC. Table 1 summarizes the molecular characteristics of the PEO-Br macroinitiator and the PEO-*b*-PNIPAM. The ^{1}H NMR spectrum in Fig. 1 reveals that the hydroxyl group of PEO-OH was fully esterified and the PEO-*b*-PNIPAM was synthesized successfully. Fig. 2 displays the GPC traces of the PEO-*b*-PNIPAM block polymer, revealing a narrow polydispersity (M_w/M_n) of 1.17. The PEO-*b*-PNIPAM block copolymer gives a single unimodel peak without shoulder or peak from the starting PEO-Br homopolymer, indicating that the sample consists of pure PEO-*b*-PNIPAM.

3.1.2. Wide-angle X-ray diffraction analysis

When an aqueous solution of PEO-*b*-PNIPAM was added to an aqueous solution of α-CD under stirring at room temperature, the solution gradually turned turbid, indicating the formation of ICs between the PEO-*b*-PNIPAM and α-CDs. The gel-like precipitates of the complexes were isolated through centrifugation and washed with a small amount of water to remove uncomplexed α-CD and free PEO-*b*-PNIPAM.

The crystalline structure of the α-CD/PEO-*b*-PNIPAM IC was established by wide-angle X-ray diffraction (WXRD) studies. Fig. 3 displays the WAXD patterns of the PEO-Br, PEO-*b*-PNIPAM, α-CD/PEO-*b*-PNIPAM IC, and uncomplexed α-CD recorded at room temperature. The major characteristic peaks for the crystalline phase of PEO-Br (Fig. 3a) appear at values of 19.4 and 23.5°, whereas the PEO-*b*-PNIPAM (Fig. 3b) displays only two broad amorphous diffuse peaks. The absence of these two characteristic

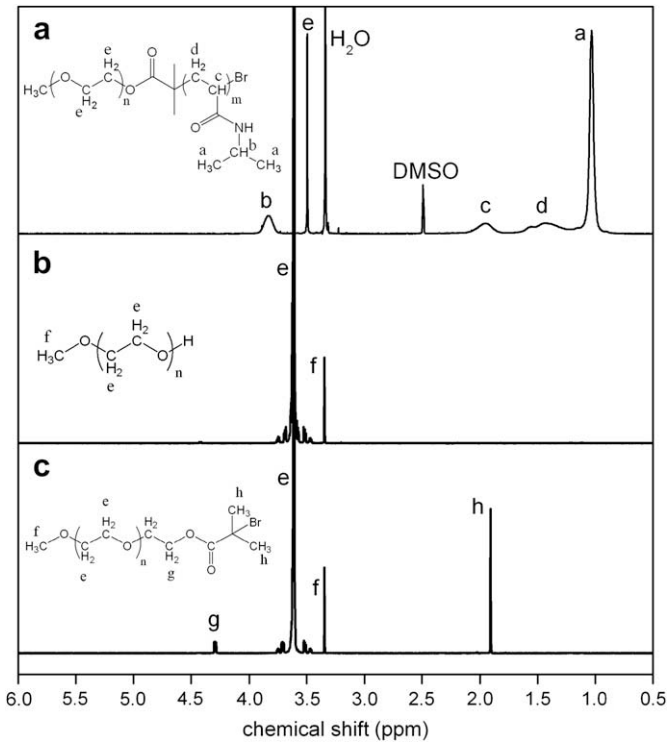

Fig. 1. ^{1}H NMR spectra of (a) PEO-*b*-PNIPAM in DMSO-d_6, (b) PEO-OH in $CDCl_3$, and (c) PEO-Br in $CDCl_3$.

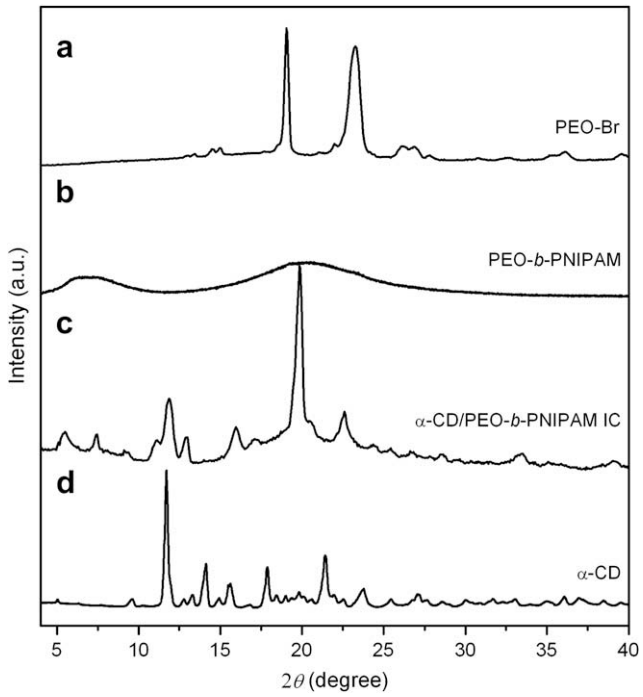

Fig. 3. WAXD profiles of (a) PEO-Br, (b) PEO-*b*-PNIPAM, (c) α-CD/PEO-*b*-PNIPAM IC, and (d) α-CD.

peaks for PEO-Br indicates that the PNIPAM segment hindered and inhibited the crystalline phase of PEO. The diffraction pattern of the α-CD/PEO-*b*-PNIPAM IC (Fig. 3c) is substantially different from those of the uncomplexed α-CD and the PEO-*b*-PNIPAM, strongly supporting the formation of ICs between the α-CD and block copolymer units. The strong peak at a value of 2θ of 20.0° (210) in the WAXD pattern of the α-CD/PEO-*b*-PNIPAM IC is characteristic of α-CD-based IC crystals adopting a channel-type structure [22,28–32]. Moreover, the prominent peaks observed at ca. 7.6° (100), 12.8° (110), 20.0° (210), and 22.6° (300) resulted from hexagonal packing of the α-CD-based IC crystals [22,33,34]. In addition, a relative weak amorphous hump at a value of 2θ from 15° to 25° is probably attributed to the PNIPAM block of the α-CD/PEO-*b*-PNIPAM IC. It was well known that the cross-sectional areas of the polymers are closely correlated to the cavity size of the CDs with which they form ICs [35]. The PEO chain is able to penetrate the α-CD cavity, but not for the PNIPAM chain because of the steric hindrance of the *N*-isopropyl amide side groups. Thus, the presence of the hump at 15–25° suggests that the phase of PNIPAM block in block copolymer remains amorphous without forming crystalline ICs with the α-CD.

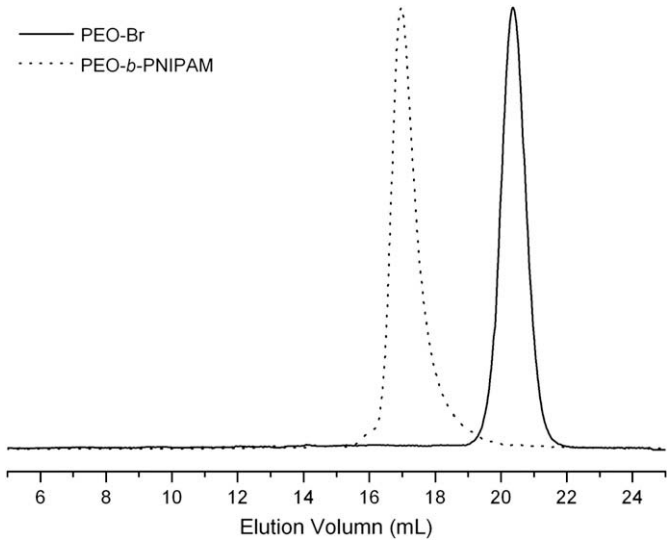

Fig. 2. GPC traces (RI detector signal) of PEO-Br and PEO-*b*-PNIPAM.

3.1.3. *Solid state ^{13}C CP/MAS NMR*

Solid state ^{13}C CP/MAS NMR spectroscopy provided additional information regarding the structure of α-CD/PEO-*b*-PNIPAM IC. Fig. 4 displays ^{13}C CP/MAS NMR spectra of α-CD, PEO-*b*-PNIPAM, and α-CD/PEO-*b*-PNIPAM IC. The α-CD molecule is known to assume a less symmetrical conformation in the uncomplexed crystalline state. In this case, the ^{13}C NMR spectrum of α-CD presents multiple resolved lines because of the C1 and C4 resonances from each of the six α-1,4-linked glucose residues, as shown in Fig. 4c [34]. Especially, resonances for C1 and C4 adjacent to a single conformationally strained glycosidic linkage are observed in the spectrum [20,36]. In contrast, the ^{13}C NMR spectrum of α-CD/PEO-*b*-PNIPAM IC (Fig. 4a) displays each C1–C6 atom of α-CD as a single unresolved resonance, indicating that the α-CD molecules adopt a symmetrical conformation and thus each glucose unit experiences a similar environment [32]. The ^{13}C CP/MAS NMR spectra provide further evidence for the formation of ICs between the α-CD and PEO-*b*-PNIPAM.

3.1.4. *^{1}H NMR spectroscopy*

The composition of α-CD/PEO-*b*-PNIPAM IC can be determined by ^{1}H NMR spectroscopy. Fig. 5 displays the ^{1}H NMR spectra of the α-CD, PEO-*b*-PNIPAM, and α-CD/PEO-*b*-PNIPAM IC. The PEO-*b*-PNIPAM chain of the α-CD/PEO-*b*-PNIPAM IC (Fig. 5a) is identical to the original PEO-*b*-PNIPAM chain in terms of the molecular weight and block lengths. We determined the ratio of the ingredients in

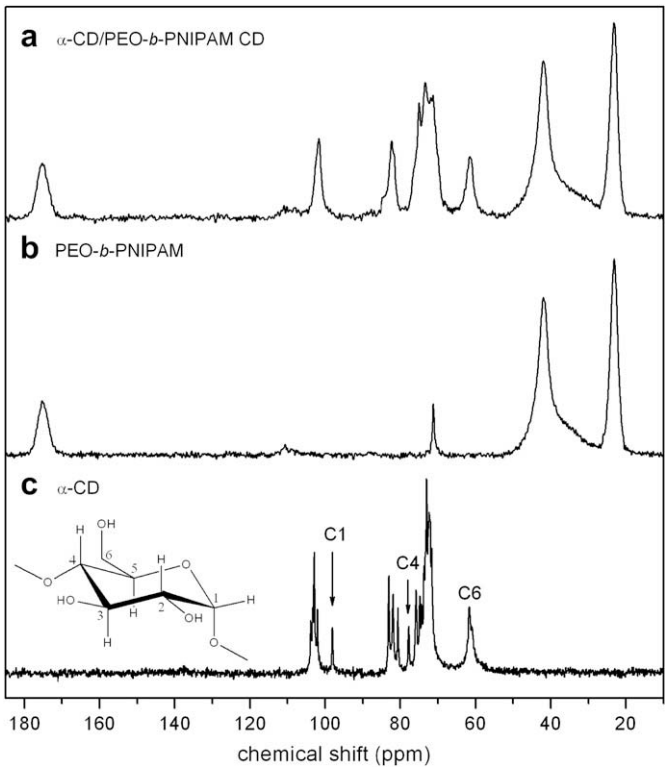

Fig. 4. ^{13}C CP/MAS NMR spectra of (a) α-CD/PEO-*b*-PNIPAM IC, (b) PEO-*b*-PNIPAM, and (c) α-CD. The arrows highlight resolved resonances for the C-1 and C-4 atoms adjacent to a single conformationally strained glycosidic linkage.

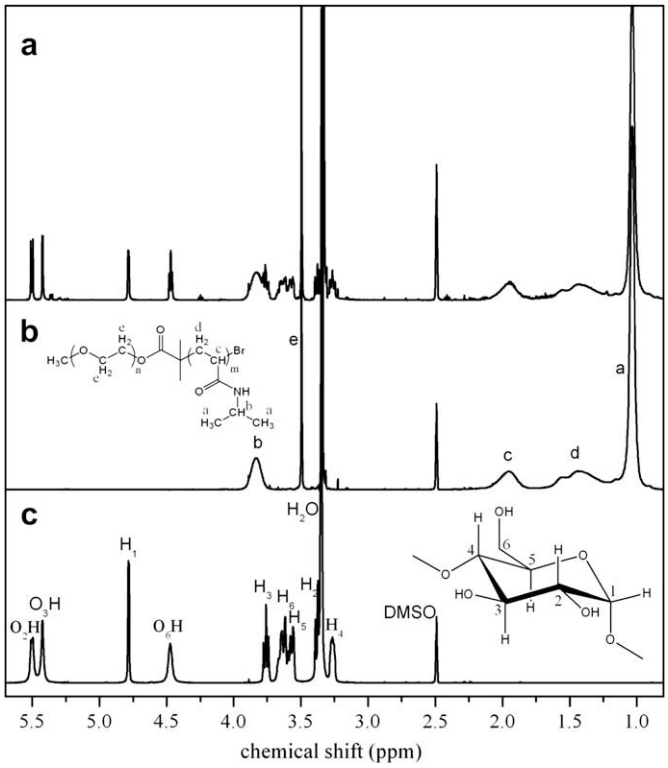

Fig. 5. ^{1}H NMR spectra of (a) α-CD/PEO-*b*-PNIPAM IC, (b) PEO-*b*-PNIPAM, and (c) α-CD in DMSO-d_6.

Table 2
Composition and stoichiometry of the α-CD/PEO-*b*-PNIPAM IC (PEO repeat units/α-CD).

Composition	Stoichiometry[a] (PEO repeat units: α-CD) of ICs	Average number of threaded α-CD units on a single chain	Coverage of PEO repeat units (%)
α-$CD_{13.7}$/PEO_{45}-*b*-$PNIPAM_{128}$	3.3	13.7	61

[a] Stoichiometry of α-CD/PEO-*b*-PNIPAM IC was determined from ^{1}H NMR spectroscopy.

α-CD/PEO-*b*-PNIPAM IC by comparing the integral intensities of the peaks for α-CD with that for PEO-*b*-PNIPAM. Table 2 lists the average number of threaded α-CD units on a single chain of the α-CD/PEO-*b*-PNIPAM IC. An ideal stoichiometry of the PEO/α-CD ICs is 2:1 (i.e., PEO repeat units to α-CD) [28,37], while the EO/α-CD molar ratio of the α-CD/PEO-*b*-PNIPAM IC is 3.3, suggesting that some of EO units are free from inclusion. It was known that the threading of α-CD units onto polymer segments is generally a reversible process [9,38–40]. Harada and Kamachi reported that the relative unthreaded cyclodextrins increased with increase in the guest polymer molecular weight. A full or near full coverage of the PEO homopolymer back bones with $M_n = 0.6$–3k by α-CD has been previously demonstrated. In this system, the M_n of the PEO block was 2k but PNIPAM block is bonded and blocked to one end of the α-CD/PEO assembly so that the α-CD can only threaded by another end of the block copolymer. Furthermore, the washing of the starting precipitate with water results in partial dissolution and dissociation of α-CD to the α-CD/PEO ICs. These effects impede complete threading and led to the stoichiometry higher than 2:1 for the α-CD/PEO ICs.

3.1.5. Thermal stability of the α-CD/PEO-b-PNIPAM IC

The thermal stability of the α-CD/PEO-*b*-PNIPAM IC was investigated by the TGA and compared with uncomplexed α-CD and the starting block copolymer. Fig. 6 displays TGA measurements of

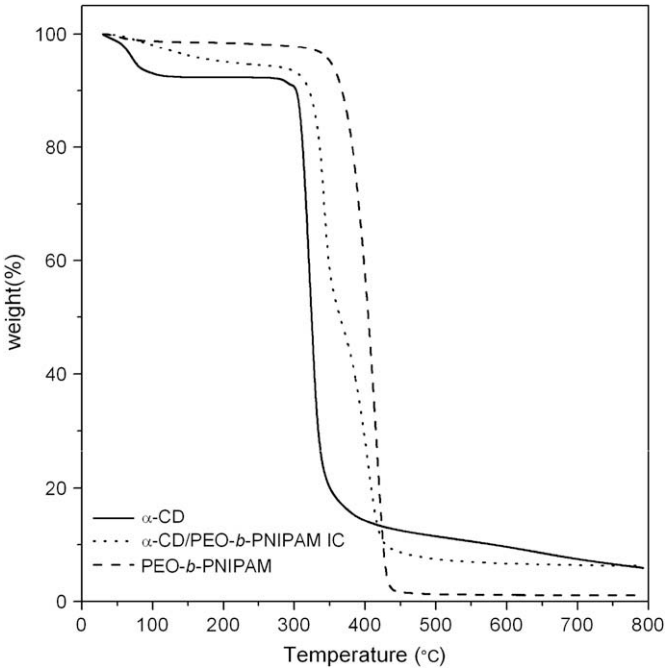

Fig. 6. TGA curves obtained at a heating rate of 20 °C/min under a nitrogen atmosphere for α-CD, PEO-*b*-PNIPAM, and α-CD/PEO-*b*-PNIPAM IC.

Table 3
Thermal properties of the PEO, PNIPAM, PEO-*b*-PNIPAM, and α-CD/PEO-*b*-PNIPAM IC.

Sample	Composition of PNIPAM[a] (wt%)	α-CD (wt%)		T_g (°C)	T_d[a] (°C)
		^{1}H NMR	TGA		
PNIPAM	100			137	
α-CD					302
PEO-*b*-PNIPAM	87			117	367
α-CD/PEO-*b*-PNIPAM IC	49	44	47	125	320

[a] Temperatures at which 10% of mass loss has occurred from TGA curves.

α-CD, PEO-*b*-PNIPAM, and α-CD/PEO-*b*-PNIPAM IC recorded at temperatures up to 800 °C. Unlike the α-CD and the free PEO-*b*-PNIPAM, the α-CD/PEO-*b*-PNIPAM IC undergoes two-step thermal degradation. The first and second steps can be attributed mainly to the decomposition of the α-CD and PEO-*b*-PNIPAM units. Table 3 summarizes thermal properties of pure PNIPAM, PEO-*b*-PNIPAM, and α-CD/PEO-*b*-PNIPAM IC. As a representative example, the onset decomposition temperatures (T_d), reflecting 10% mass losses [41] for α-CD, PEO-*b*-PNIPAM, and α-CD/PEO-*b*-PNIPAM IC are 302, 367 and 320 °C, respectively. Thus, the thermal stability of the threaded α-CD units in the α-CD/PEO-*b*-PNIPAM IC is higher than that of pure α-CD, implying that the α-CD unit is more stable by complexing with PEO. Moreover, the weight ratio between α-CD and the copolymer in the α-CD/PEO-*b*-PNIPAM IC can be estimated approximately from the two-step weight loss of the TGA thermogram, which is in quite good agreement with that calculated using ^{1}H NMR as shown in Table 3.

3.2. Supramolecular structures of self-assembled inclusion complexes in the bulk state

3.2.1. Differential scanning calorimetry

DSC analysis was carried out to gather more information on determining the self-assembly behavior of the α-CD/PEO-*b*-PNIPAM IC. Fig. 7 shows the conventional second run DSC thermograms of PEO-Br, PNIPAM, PEO-*b*-PNIPAM, and α-CD/PEO-*b*-PNIPAM IC. For the thermogram of PEO-Br, a distinct endothermic peak at 54 °C is corresponding to the melting temperature (T_m) of the crystalline PEO. The T_m and the heat fusion of the crystalline PEO of the PEO-*b*-PNIPAM are fully depressed, confirming that the presence of PNIPAM chain in the copolymer disturbs and inhibits the crystallization of PEO block. Moreover, the DSC thermogram of PEO-*b*-PNIPAM shows single glass transition temperature (T_g) at 117 °C, which is lower than the T_g of the pure PNIPAM at 137 °C. This T_g of the PEO-*b*-PNIPAM is quite consistent with that estimated from the Gordon–Taylor equation (115 °C) [42]. This result indicates that this PEO-*b*-PNIPAM is almost miscible in its bulk state. On the other hand, the T_g of the α-CD/PEO-*b*-PNIPAM IC is 125 °C which is slightly higher than the T_g of PEO-*b*-PNIPAM, indicating that the amorphous PNIPAM block is not covered by α-CD. The α-CD units are looped tightly around the PEO chains and reorganized into the IC crystals. Meanwhile, the self-assembly of the ICs formed between the PEO and α-CD units tends to repel the PNIPAM to form own IC crystal domains. Thus, the phase separated PNIPAM domain of the α-CD/PEO-*b*-PNIPAM IC shifts its T_g higher, close to the pure PNIPAM homopolymer. Combining results from WAXD and DSC, we can conclude that phase separation occurs through the formation of ICs between α-CD units and PEO-*b*-PNIPAM.

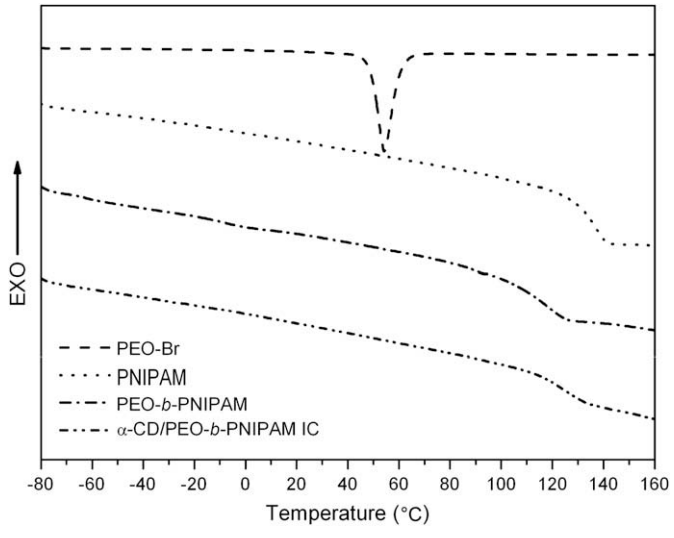

Fig. 7. DSC thermograms of the PEO-Br, PNIPAM, PEO-*b*-PNIPAM, and α-CD/PEO-*b*-PNIPAM IC.

3.2.2. SAXS analyses

To further characterize the microdomain structure of the α-CD/PEO-*b*-PNIPAM IC, SAXS measurements were performed to determine the morphological changes induced through phase separation of the crystalline α-CD/PEO ICs and the coil segments of PNIPAM chains. Fig. 8a reveals that SAXS scattering from free α-CD and PEO-*b*-PNIPAM decreases monotonically without any peak, implying the absence of a self-assembled structure. The SAXS profile of the α-CD/PEO-*b*-PNIPAM IC (Fig. 8b) shows well-defined lattice peaks with relative positions (i.e., 1:2:3) relevant to the lamellar morphology of alternating α-CD/PEO ICs and PNIPAM layers. The lamellar distance (L) of the α-CD/PEO-*b*-PNIPAM IC calculated from the first peak position in the SAXS profile using the expression $2\pi/Q_c$ is 31.4 nm. According to the WAXD and DSC results discussed above, these α-CD units are stacked along a PEO chain axis to form stiff rods in the vertical direction and these rods are then aligned hexagonally in the horizontal direction. The α-CD/PEO-*b*-PNIPAM IC tends to form two phase-separated microdomains with an altering layer of the crystal plate of the α-CD/PEO ICs and the amorphous phase of PNIPAM block. These results indicate that the α-CD/PEO ICs of the α-CD/PEO-*b*-PNIPAM IC are the hexagonal component in the lamellar morphology.

3.2.3. Supramolecular self-assembly structure of α-CD/PEO-b-PNIPAM IC

The one-dimensional correlation function can determine more structural information in this α-CD/PEO-*b*-PNIPAM IC, including the most probable average long period L, the average crystalline lamellar thickness L_c, and the average interlamellar amorphous layer thickness L_a ($L_a = L - L_c$). Fig. 9 shows the one-dimensional correlation function calculated from the SAXS data of the α-CD/PEO-*b*-PNIPAM IC. The average long period of the α-CD/PEO-*b*-PNIPAM IC is 32.2 nm, which is comparable with the interlamellar distance determined by the first peak position of the SAXS profile. Based on the self-correlation triangle method, the mean thickness of L_1 is 13.1 nm, so the mean thickness of L_2 is 19.1 nm ($32.2 - 13.1 = 19.1$ nm). However, the correlation function is unable to directly distinguish which thickness value represents the length of the crystalline and the amorphous phase. Generally, when a polymeric guest is included into the α-CD cavity, a number of hydrogen bonds are established between the hydroxyl groups situated along the rim of the α-CD, and then produce large aggregates of crystal plates [8,43]. Fleury et al. employed the rod-like form factor for the α-CD/PEO_{20K} ICs even though with the (33%) α-CD coverage [44]. As determined by the ^{1}H NMR spectra, the coverage

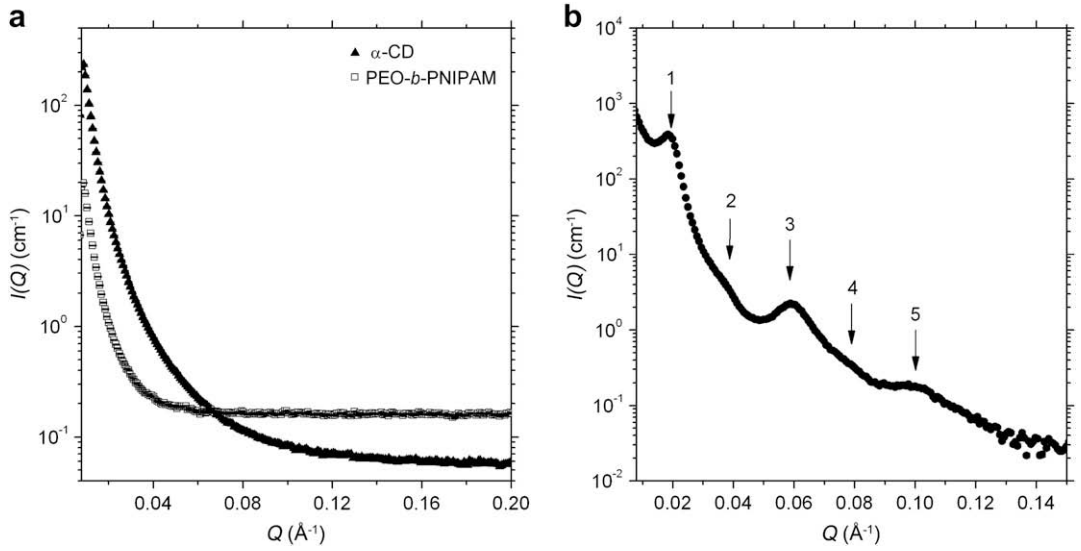

Fig. 8. Small-angle X-ray scattering intensity profiles as a function of wave vector Q for (a) α-CD, PEO-*b*-PNIPAM, and (b) α-CD/PEO-*b*-PNIPAM IC at room temperature.

of PEO repeat units for α-CD/PEO-*b*-PNIPAM IC is 61% (Table 2). Chung et al. also reported that the irregularly interacted hydrogen bonding between crystals in ICs can be broken and reorganized during THF treatment, but not the hydrogen bonding formed between the regularly arranged crystals and the adjacent CDs that threaded on a single chain [22,45]. The WAXD data of the THF treated α-CD/PEO-*b*-PNIPAM IC shows somewhat more vivid peaks than the α-CD/PEO-*b*-PNIPAM IC before THF treatment (Fig. 10), indicating the increase in the crystalline size and regularity of the α-CD/PEO ICs in the α-CD/PEO-*b*-PNIPAM IC. On the other hand, the SAXS profile of the α-CD/PEO-*b*-PNIPAM IC before THF treatment also shows broad and invisible scattering peaks (Fig. 11), suggesting a more disordered structure than that of the THF treated α-CD/PEO-*b*-PNIPAM IC. Based on these results, we assume that α-CD units on a single PEO chain are drawn into close proximity and interact with each other through hydrogen bonding after THF treatment. The irregular IC crystals are then reorganizing to more stable and well-ordered hexagonally packed crystals. The free uncovered PEO segments are situated closest to the surfaces of the α-CD hydrogen-bonded stacks or columns. Since the average number of threaded α-CD units on a single chain is determined from ^{1}H NMR spectra, the average length of the single IC segment for α-CD/PEO-*b*-PNIPAM IC can be calculated (the number of threaded CDs×the CD torus heights, $13.6 \times 0.78 = 10.6$ nm). Therefore, the mean thickness of L_1 ($L_1 = L_c = 13.1$ nm) calculated from the self-correlation function is more reasonably attributed to the thickness of the α-CD/PEO ICs layer.

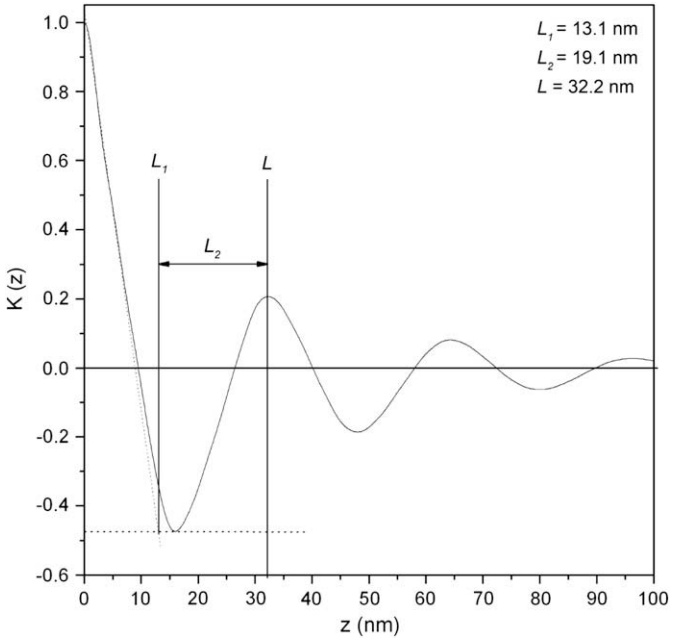

Fig. 9. One-dimensional correlation function derived from SAXS measurements of α-CD/PEO-*b*-PNIPAM IC.

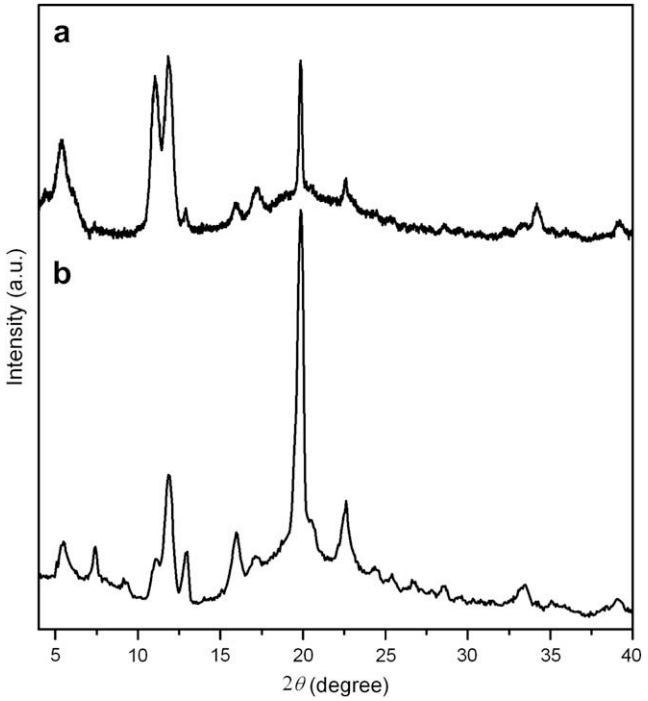

Fig. 10. WAXD profiles of α-CD/PEO-*b*-PNIPAM IC (a) before and (b) after THF treatment.

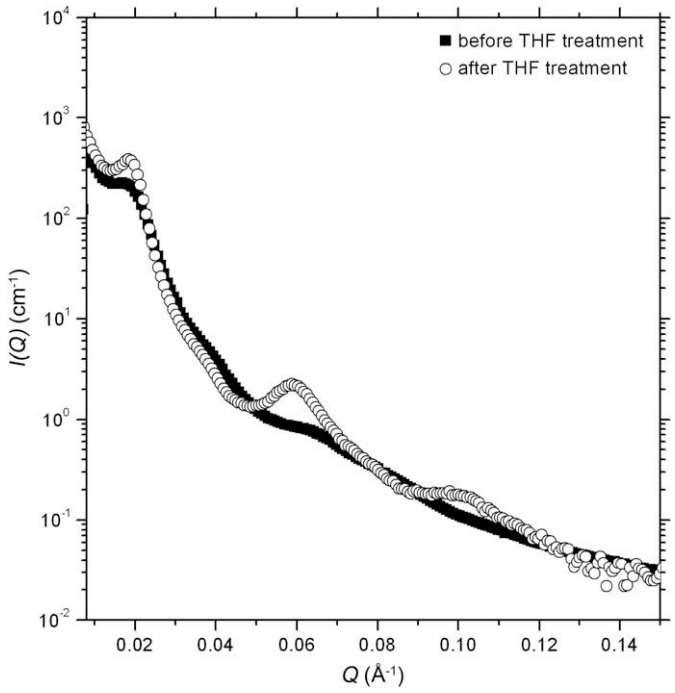

Fig. 11. SAXS intensity profiles as a function of wave vector Q for α-CD/PEO-*b*-PNIPAM IC before and after THF treatment.

Regarding to the amorphous phase, the unincluded PEO/PNIPAM chains dangle from only one surface of the α-CD/PEO IC crystals. For α-CD, the diameter of the outer periphery is 14.6 Å [46]. Therefore, the grafting density (σ) and the average distance between grafting sites (D) of the free PEO and PNIPAM chains could be calculated from the surface area of hexagonal packed ICs crystal plate ($\sigma \sim 0.27$ chain/nm^2 and $D \sim 1.92$ nm, respectively). When flexible polymers such as PNIPAM are grafted to a surface, brush formation begins when D is smaller than the Flory radius $R_F = aN^{3/5}$ [47,48], where a is the effective segment length, assumed to be 3 Å [49], and N is the number of segment. The Flory radius of PNIPAM segment with $M_n = 14{,}500$ ($n = 128$) is 5.51 nm. The D/R_F ratios for α-CD/PEO-*b*-PNIPAM IC is 0.35, indicating that PNIPAM chains show the dry brush configuration. The amorphous PNIPAM chains would be more extended from their random coiling value and do not interpenetrate, because of the high density of PEO/PNIPAM chains dangling from the crystal α-CD/PEO ICs plate. Furthermore, the amorphous largely PNIPAM brush is from the crystal surface by the unincluded and inherently flexible PEO segments, which is consist with its T_g that is low than observed from the PNIPAM homopolymer. Thus, the 19.1 and 13.1 nm thickness are attributed to the amorphous phase of unincluded PEO/PNIPAM and the layer of the α-CD/PEO ICs crystals, respectively.

Recently, the lamellar structures were also observed in the multi-arm hyperbranched polyether IC or the P(EO-*r*-PO)-*b*-PBLG IC with α-CDs [12,25]. However, these IC-based polymers revealed only a broader peak at low scattering angles, indicating a poorly ordered lamellar organization. In contrast, the SAXS profile from the α-CD/PEO-*b*-PNIPAM IC reveals five lamellar scattering orders, suggesting that the morphology of the α-CD/PEO-*b*-PNIPAM IC is arranged in long-range-ordered lamellar assembly. To the best of our knowledge, this is the first report that shows a long-range-ordered lamellar assembly of IC-based block copolymer. Finally, we concluded that the structure of the α-CD/PEO-*b*-PNIPAM IC is the lamellar structure consisting of two layers: one layer formed by the α-CD/PEO ICs with rod-like conformation, arranged on a hexagonal

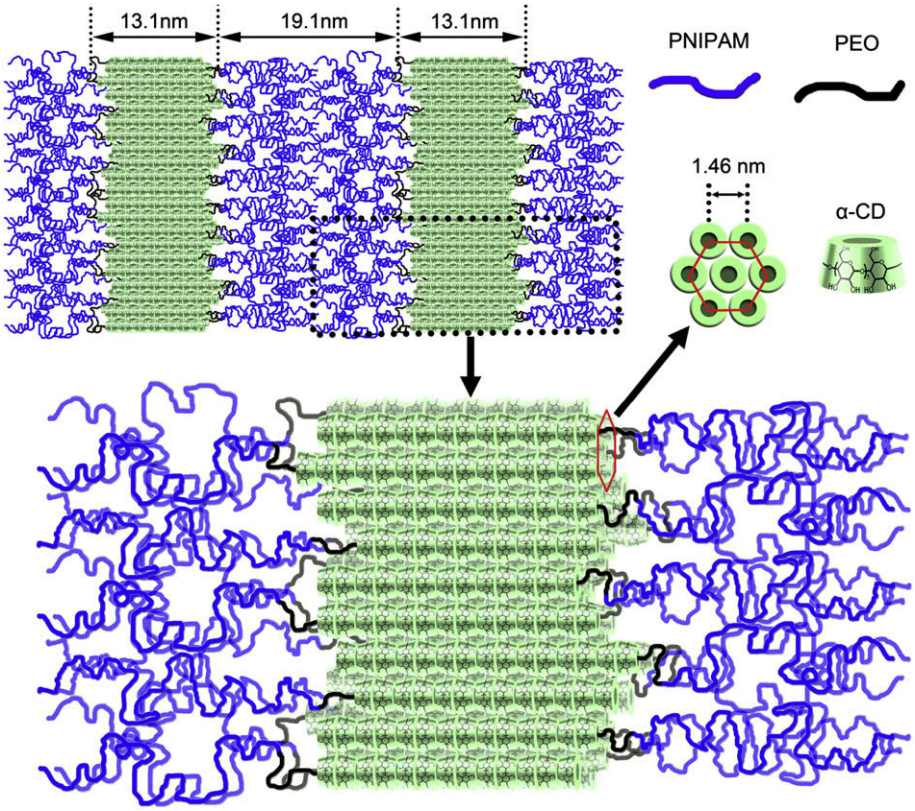

Scheme 2. Schematic representation of the self-assembly of the α-CD/PEO-*b*-PNIPAM IC.

array, perpendicular to the interface; and the other layer formed by the free PEO/PNIPAM with brush conformation.

From the combined results of the WAXD, SAXS, and DSC analyses, we conclude that non-covalent interactions between the α-CD and PEO units, hydrogen bonding between the individual ICs, and the reorganization of the α-CD/PEO-*b*-PNIPAM IC play important roles in the formation of the hexagonal in lamellar architectures. When α-CD units are added to the PEO-*b*-PNIPAM, molecular recognition and the formation of IC crystals induce the phase separation, thereby changing the solid morphology of the system relative to those of the PEO-*b*-PNIPAM. Scheme 2 presents a possible structure for the ICs formed from α-CD units and the PEO-*b*-PNIPAM block copolymer: a lamellar structure possessing alternating layers of (i) α-CD/PEO ICs with hexagonally packed plates and (ii) amorphous phase of unincluded PEO/PNIPAM with brush conformation.

4. Conclusions

This paper describes the preparation and the long-range-ordered supramolecular organization of α-CD/PEO-*b*-PNIPAM IC. The PEO-*b*-PNIPAM block copolymer was successfully synthesized through atom transfer radical polymerization and characterized by GPC and ^{1}H NMR spectroscopy. The α-CD/PEO-*b*-PNIPAM IC comprises coil segment of unincluded PEO/PNIPAM and rod segment of included PEO that was thread through α-CD units to form inclusion complexes on the other. For the self-assembled structure, the DSC, XRD, and simultaneous SAXS/WAXS data suggest that the α-CD/PEO-*b*-PNIPAM IC is phase-separated into long-range-ordered lamellar structure containing alternating layers of α-CD/PEO ICs with hexagonally packed plates and amorphous phase of unincluded PEO/PNIPAM with brush conformation.

Acknowledgement

We thank Dr. U.S. Jeng for the help with the simultaneous SAXS measurements, which were conducted at beamline BL17B3 of the National Synchrotron Radiation Research Center (NSRRC), Taiwan.

References

[1] Harada A, Li J, Kamachi M. Nature 1993;364(6437):516–8.
[2] Gerhard W. Angew Chem Int Ed Engl 1994;33(8):803–22.
[3] Li X, Li J, Leong KW. Macromolecules 2003;36(4):1209–14.
[4] Bender ML, Komiyama M. Cyclodextrin chemistry. Berlin: Springer-Verlag; 1978.
[5] Rusa CC, Bullions TA, Fox J, Porbeni FE, Wang X, Tonelli AE. Langmuir 2002;18(25):10016–23.
[6] He LH, Huang J, Chen YM, Liu LP. Macromolecules 2005;38(8):3351–5.
[7] Harada A, Li J, Kamachi M. Nature 1994;370(6485):126–8.
[8] Ceccato M, Lo Nostro P, Baglioni P. Langmuir 1997;13(9):2436–9.
[9] Loethen S, Kim J-M, Thompson DH. Polym Rev 2007;47(3):383–418.
[10] Harada A, Kamachi M. Macromolecules 1990;23(10):2821–3.
[11] Chan SC, Kuo SW, Chang FC. Macromolecules 2005;38(8):3099–107.
[12] Lee HF, Sheu HS, Jeng US, Huang CF, Chang FC. Macromolecules 2005;38(15):6551–8.
[13] Tonelli AE. Polymer 2008;49(7):1725.
[14] Li J, Ni X, Leong KW. Angew Chem Int Ed 2003;42(1):69–72.
[15] Rusa CC, Tonelli AE. Macromolecules 2000;33(15):5321–4.
[16] Shuai X, Porbeni FE, Wei M, Bullions T, Tonelli AE. Macromolecules 2002;35(8):3126–32.
[17] Jia X, Wang X, Tonelli AE, White JL. Macromolecules 2005;38(7):2775–80.
[18] Choi HS, Lee SC, Yamamoto K, Yui N. Macromolecules 2005;38(23):9878–81.
[19] Dong T, Kai W, Pan P, Cao A, Inoue Y. Macromolecules 2007;40(20):7244–51.
[20] Li J, Ni X, Zhou Z, Leong KW. J Am Chem Soc 2003;125(7):1788–95.
[21] Chan SC, Kuo SW, Sheu HS, Lin HM, Lee HF, Chang FC. J Polym Sci Part A Polym Chem 2007;45(1):125–35.
[22] Chung JW, Kang TJ, Kwak SY. Macromolecules 2007;40(12):4225–34.
[23] Zhang S, Yu ZJ, Govender T, Luo HY, Li BJ. Polymer 2008;49(15):3205.
[24] Araki J, Ito K. Polymer 2008;48(24):7139.
[25] Zhu X, Chen L, Yan D, Chen Q, Yao Y, Xiao Y, et al. Langmuir 2004;20(2):484–90.
[26] Xia J, Zhang X, Matyjaszewski K. Macromolecules 1999;32(10):3531–3.
[27] Zhang W, Shi L, Ma R, An Y, Xu Y, Wu K. Macromolecules 2005;38(21):8850–2.
[28] Harada A, Li J, Kamachi M. Macromolecules 1993;26(21):5698–703.
[29] Rusa CC, Tonelli AE. Macromolecules 2000;33(5):1813–8.
[30] Harada A, Okada M, Li J, Kamachi M. Macromolecules 1995;28(24):8406–11.
[31] Li J, Li X, Zhou Z, Ni X, Leong KW. Macromolecules 2001;34(21):7236–7.
[32] Huh KM, Ooya T, Sasaki S, Yui N. Macromolecules 2001;34(8):2402–4.
[33] Hwang MJ, Bae HS, Kim SJ, Jeong B. Macromolecules 2004;37(24):8820–2.
[34] Harada A. Coord Chem Rev 1996;148:115–33.
[35] Harada A. Adv Polym Sci 1997;133:141–91.
[36] Gidley MJ, Bociek SM. J Am Chem Soc 1988;110(12):3820–9.
[37] Harada A, Li J, Kamachi M. Macromolecules 1994;27(16):4538–43.
[38] Agrawal YK, Sharma CR. Rev Anal Chem 2005;24(1):35–74.
[39] Wenz G, Han BH, Muller A. Chem Rev 2006;106(3):782–817.
[40] Harada A, Hashidzume A, Takashima Y. Adv Polym Sci 2006;201:1–43.
[41] Arnal ML, Balsamo V, Lopez-Carrasquero F, Contreras J, Carrillo M, Schmalz H, et al. Macromolecules 2001;34(23):7973–82.
[42] Gordon M, Taylor JS. J Appl Chem 1952;2:493.
[43] Miyake K, Yasuda S, Harada A, Sumaoka J, Komiyama M, Shigekawa H. J Am Chem Soc 2003;125(17):5080–5.
[44] Fleury G, Brochon C, Schlatter G, Bonnet G, Lapp A, Hadziioannou G. Soft Matter 2005;1(5):378–85.
[45] Chung JW, Kang TJ, Kwak SY. Langmuir 2007;23(24):12366–70.
[46] Szejtli J. Chem Rev 1998;98(5):1743–54.
[47] Lyngs Hansen P, Cohen JA, Podgornik R, Parsegian VA. Biophys J 2003;84(1):350–5.
[48] Zhu X, Yan C, Winnik FM, Leckband D. Langmuir 2007;23(1):162–9.
[49] Carey FA. Organic chemistry. 2nd ed. New York: McGraw-Hill; 1992.